

Modeling $\delta^{18}\text{O}$ in tropical precipitation and the surface ocean for present-day climate

J. Brown,^{1,2} I. Simmonds,¹ and D. Noone³

Received 16 November 2004; revised 22 October 2005; accepted 1 December 2005; published 7 March 2006.

[1] The Melbourne University atmospheric general circulation model with stable water isotope tracers is used to examine the variability of isotopic ratios of precipitation and the surface ocean in the tropics for present-day (1950–1999) climate. Surface ocean isotopic ratios are simulated interactively using a one-dimensional scheme that reproduces key features of the observed tropical isotopic spatial distribution and seasonal and interannual variability. The seasonal and interannual variability of modeled isotopic ratios of tropical precipitation is strongly associated with changes in precipitation amount, in agreement with previous isotopic modeling studies. Modeled isotopic ratios of both precipitation and surface ocean water respond to El Niño–Southern Oscillation (ENSO), although the spatial patterns of ENSO and monsoon isotopic responses differ from observations because of biases in the simulated tropical climate. The model captures the dependence of the interannual variability of precipitation isotopic ratios over the tropical Andes on local temperature and precipitation variability and moisture balance over the Amazon basin but fails to reproduce a significant ENSO precipitation or isotope signal over this region. Modeled precipitation isotopic ratios are significantly correlated with local precipitation amount but not with local or regional temperature at Tibetan Plateau ice core sites on interannual timescales, in disagreement with the interpretation of these ice core records as temperature proxies. Surface ocean isotopic ratios are used to calculate modeled “coral,” isotopic ratios which are compared with modern coral records, reproducing observed interannual variability where precipitation is well simulated.

Citation: Brown, J., I. Simmonds, and D. Noone (2006), Modeling $\delta^{18}\text{O}$ in tropical precipitation and the surface ocean for present-day climate, *J. Geophys. Res.*, *111*, D05105, doi:10.1029/2004JD005611.

1. Introduction

[2] Oxygen isotope ratios in climate proxy records such as ice cores and coral and foraminiferal carbonate are used to assist in the quantitative reconstruction of tropical climate on a range of timescales. Continental and marine isotope records hold information about tropical climate variability prior to the instrumental record, and provide evidence of the tropical sensitivity to past global climate change. Tropical and subtropical ice cores provide records of precipitation isotopic ratios from sites including Huascarán and Quelccaya in Peru [Thompson *et al.*, 1985, 1995, 2000a], Sajama and Illimani in Bolivia [Thompson *et al.*, 1998; Hoffmann *et al.*, 2003; Ramirez *et al.*, 2003] in the South American Andes; Dunde, Guliya and Dasuopu on the Tibetan Plateau

[e.g., Thompson *et al.*, 1989, 1997, 2000b] and Mount Kilimanjaro [Thompson *et al.*, 2002]. Marine isotope records are used to investigate tropical climate variability such as El Niño–Southern Oscillation (ENSO) and the Asian monsoon [e.g., Cole *et al.*, 1993a; Tudhope *et al.*, 1995; Charles *et al.*, 1997, 2003; Tudhope *et al.*, 2001; Cobb *et al.*, 2003], as well as to estimate changes in sea surface temperature (SST), ocean isotopic ratio and salinity on glacial timescales [e.g., Koutavas *et al.*, 2002; Stott *et al.*, 2002; De Deckker *et al.*, 2003]. The oxygen isotopic composition of tree cellulose is also used to reconstruct climate trends [e.g., Saurer *et al.*, 2002] and tropical climate variability [e.g., Poussart *et al.*, 2004].

[3] Measurements of isotopic ratios of precipitation (generally expressed in “delta” notation: $\delta^{18}\text{O} = (R_{\text{sample}}/R_{\text{VSMOW}} - 1) \times 1000$ for oxygen isotopes, where R_{VSMOW} is the ratio of Vienna Standard Mean Ocean Water) covering more than fifty years are now available from the Global Network of Isotopes in Precipitation (GNIP) maintained by the International Atomic Energy Agency (available online at <http://isohis.iaea.org>). At high latitudes, the extent of isotopic depletion of precipitation is observed to be correlated with the local surface or condensation temperature (the “temperature effect”) [Dansgaard, 1964] although a number of studies have shown that this rela-

¹School of Earth Sciences, University of Melbourne, Parkville, Victoria, Australia.

²Now at Centre for Global Atmospheric Modeling, Department of Meteorology, University of Reading, Reading, UK.

³Program in Atmospheric and Oceanic Sciences and Cooperative Institute for Research in Environmental Sciences, University of Colorado, Boulder, Colorado, USA.

relationship may not hold under certain paleoclimate conditions [e.g., *Charles et al.*, 1994; *Brown and Simmonds*, 2004; *Noone and Simmonds*, 2004]. In the tropics, the isotopic ratio of precipitation is influenced by local temperature as well as precipitation amount, where isotopic distillation is associated with the rainout of atmospheric moisture locally and during transport (the “amount effect”) [e.g., *Dansgaard*, 1964; *Araguas-Araguas et al.*, 1998]. The complexity of the tropical precipitation isotope signal means that the interpretation of isotopic proxy records such as tropical and subtropical ice cores remains the subject of some debate [e.g., *Pierrehumbert*, 1999; *Thompson et al.*, 2000b, 2003; *Ramirez et al.*, 2003].

[4] Ocean water isotopic measurements have also been obtained over several decades from the GEOSECS survey and other data sets now collated in the NASA GISS Global Seawater Oxygen-18 Database (available at <http://www.giss.nasa.gov/data/o18data>) as described by *Bigg and Rohling* [2000]. The isotopic ratio of ocean water is known to be controlled by the balance between evaporation, which enriches ocean water in the heavy isotopic species, and precipitation, which is generally isotopically light relative to ocean water, as well as factors including ocean transport and upwelling, river runoff and sea ice formation [e.g., *Craig and Gordon*, 1965]. As these factors also influence salinity, ocean isotopic ratios are closely related to salinity. Marine carbonates such as coral and foraminifera incorporate oxygen from ocean water with a dependence on the isotopic ratio of local ocean water, as well as a biological fractionation with ocean temperature or SST. The reconstruction of salinity and SST from marine isotope records therefore requires the separation of the two components of the isotope record [e.g., *Wellington et al.*, 1996; *Crowley et al.*, 1999]. The reconstruction of paleosalinity using present-day salinity– $\delta^{18}\text{O}$ regressions may also involve large uncertainties because of factors such as differences between temporal and spatial salinity– $\delta^{18}\text{O}$ slopes and changes in advection and mixing of water masses [*Rohling and Bigg*, 1998; *Schmidt*, 1999a].

[5] One approach to improve the understanding of climate controls on isotopic ratios is to incorporate stable water isotope tracers into General Circulation Models (GCMs). Stable water isotope tracers have been incorporated into the LMD [*Joussaume et al.*, 1984], GISS [*Jouzel et al.*, 1987], ECHAM [*Hoffmann et al.*, 1998] and GENESIS [*Mathieu et al.*, 2002] atmospheric models as well as the Melbourne University GCM (MUGCM) [*Noone and Simmonds*, 2002] used in this study. The controls on seasonal and interannual precipitation isotopic variability in the tropics have been investigated in previous modeling studies with the GISS model [*Cole et al.*, 1993b, 1999], the ECHAM model [*Hoffmann et al.*, 1998] and the MUGCM [*Noone and Simmonds*, 2002]. These studies identified a strong relationship between precipitation amount and precipitation $\delta^{18}\text{O}$ in the tropics, with an ENSO signal in tropical precipitation isotopic ratios on interannual timescales. *Schmidt* [1998] incorporated oxygen isotope tracers into the GISS ocean GCM (OGCM). *Delaygue et al.* [2000, 2001] investigated changes in the relationship between salinity and ocean isotopic ratios using both a simple box model and the OPA OGCM with isotopic tracers and *Wadley et al.* [2002] modeled present and last glacial

maximum climate using the SEA OGCM with isotopic tracers.

[6] Modeling studies have also attempted to explicitly simulate the isotope signal in proxy records, and to investigate the relationships used in paleoclimate reconstructions from such records. *Hoffmann et al.* [2003] and *Hoffmann* [2003] compared isotopic ratios of precipitation over the South American Andes simulated by the ECHAM-4 model with records from the Huascarán, Quelccaya, Sajama and Illimani ice cores, from which they constructed an Andean Isotope Index (AII). They found a coherent decadal time-scale signal in the ice core records which was reproduced by the model in response to ENSO-associated Amazon basin precipitation variability. *Vuille et al.* [2003a, 2003b] compared Andean ice cores with simulations using the T42 and T106 resolution versions of ECHAM-4 model and the GISS II model with increased Andean topography. They found an ENSO signal in precipitation isotopic ratios over the tropical Andes which was interpreted as the combined result of temperature, precipitation and circulation changes. *Schmidt* [1999b] estimated the isotope signal in planktonic foraminifera using ocean isotopic ratios and a forward model of the relevant isotopic fractionation and biological processes.

[7] The aim of this study is to use the MUGCM atmospheric model, incorporating a simple representation of the surface ocean isotopic budget, to simulate the distribution and variability of isotopic ratios of precipitation and the surface ocean in the tropics. We examine the impact of an interactive representation of surface ocean isotopic ratios on the atmospheric isotopic distribution and consider the benefits of the scheme for simulating marine and continental isotope records. We identify interannual variability in tropical temperature and precipitation and in isotopic ratios of precipitation and the surface ocean, and compare the simulated variability with instrumental and proxy records. We conclude with a discussion of the strengths and limitations of the approach for the simulation of stable water isotopes in the tropics for modern and past climates.

2. Model Description

2.1. Atmospheric Model

[8] The MUGCM is a spectral atmospheric model with R21 horizontal resolution (3.3° latitude \times 5.6° longitude) and nine vertical levels in sigma coordinates, described in detail by *Simmonds* [1985]. The model parameterizations include the moist convective adjustment of *Manabe et al.* [1965], prognostic cloud fraction [*Argete and Simmonds*, 1996] and a two-layer soil moisture scheme [*Deardorff*, 1977]. Moisture is advected using a semi-Lagrangian transport scheme based on *Williamson and Rasch* [1989], a technique which allows the accurate representation of water and water isotope ratios, particularly at high latitudes. All nonfrozen land surfaces are treated as bare soil whose albedo is a function of soil moisture. Snow cover is prescribed from observations for the purpose of land surface thermodynamic and albedo calculations, while the model does not include a separate snow reservoir within the hydrological scheme. Instead, frozen precipitation is treated as liquid precipitation at the land surface, and accumulates in the soil layers. River runoff is defined

as the precipitated water in excess once soil moisture reaches saturation level, which is then removed from the water budget.

[9] The model incorporates a stable water isotope tracer scheme as described by *Noone and Simmonds* [2002]. This scheme represents the isotopically heavy species of water in parallel to “normal” water in the model’s hydrologic cycle, with the inclusion of equilibrium and kinetic isotopic fractionation during phase transitions. Over land surfaces, evapotranspiration occurs without fractionation. Evaporation from ice, snow and frozen soil also occurs without fractionation as the low diffusivity of the isotopic species in the solid phase prevents isotopic exchange. Over ocean, fractionation occurs during evaporation, with kinetic effects parameterized from the surface wind speed for smooth and rough flow regimes following *Jouzel et al.* [1987]. The formation of dew and frost occurs when the evaporative flux is negative in which case fractionation is included with kinetic effects.

[10] In the model’s condensation scheme, large-scale precipitation and convective precipitation are distinguished by the existence of instability in the atmospheric column. Large-scale precipitation occurs with total equilibrium fractionation, with fractionation to liquid above -10°C and fractionation to solid below this temperature. In the case of convective precipitation, Rayleigh fractionation is applied for solid condensate (temperatures less than -10°C) and total equilibrium fractionation otherwise. For all condensation kinetic effects are included for temperatures below -20°C via the supersaturation parameterization of *Jouzel et al.* [1987]. Reevaporation of falling condensate occurs without fractionation for solid condensate, and with fractionation and kinetic effects for liquid condensate. The extent of equilibration between precipitation and the surrounding vapor is parameterized following *Hoffmann et al.* [1998] with 45% fractionation for convective precipitation (large drops) and 95% for large-scale precipitation (small drops). The isotopic tracer scheme in the model has been shown to produce a good simulation of the global distribution of precipitation $\delta^{18}\text{O}$ for the present-day climate [*Noone and Simmonds*, 2002].

2.2. Surface Ocean Scheme

[11] The version of the isotopic tracer scheme in MUGCM described by *Noone and Simmonds* [2002] used a globally uniform surface ocean isotopic ratio to determine the ratio of moisture evaporated from the ocean, as in the other isotopic atmospheric GCMs referred to above. In order to capture the spatial and temporal variability of the surface ocean isotopic composition, the approach of previous surface ocean “box” modeling studies [e.g., *Juillet-Leclerc et al.*, 1997; *Delaygue et al.*, 2000] is extended here to include an interactive surface box model. In this study, the isotopic ratio of a surface box at each ocean grid point is calculated interactively from precipitation and evaporation and the corresponding isotopic water fluxes. This surface ocean isotopic ratio can then influence the atmospheric distribution of isotopes, as well as responding to changing atmospheric fluxes.

[12] In the scheme, the depth of a surface ocean water layer Q is calculated from the difference between precipitation (P) and evaporation (E), while the equivalent isotopic

tracer water layer depth is calculated from the isotopic surface hydrologic fluxes (P_i , E_i). A damping term relaxes Q back to a mean depth h and Q_i back to a mean depth hR_{deep} (where R_{deep} is the mean deep ocean isotopic ratio) with a timescale determined by a coefficient k . The damping term parameterizes the mixing and entrainment of deeper waters into the surface layer. The time variation of the surface water and isotopic tracer layer depths is therefore given by

$$\frac{\partial Q}{\partial t} = (P - E) + k(h - Q) \quad (1)$$

$$\frac{\partial Q_i}{\partial t} = (P_i - E_i) + k(hR_{deep} - Q_i) \quad (2)$$

[13] The layer depth h and the damping timescale k were tuned to produce a mean surface ocean $\delta^{18}\text{O}$ distribution and seasonal range in agreement with the observed range of surface ocean $\delta^{18}\text{O}$ values in the tropics and midlatitudes from the Global Seawater Oxygen-18 Database. As this version of the model does not include a representation of continental snowmelt and river runoff, it is not expected to reproduce the highly depleted surface ocean isotopic values observed at high latitudes. This limitation was considered acceptable as this study focuses on isotopic variability in the tropics. The values chosen for the depth and timescales were $h = 5$ m and $k = 1.17 \times 10^{-7} \text{ s}^{-1}$. These values differ from the observed values for the mixed layer as the parameterization neglects mixing processes including horizontal advection, vertical mixing and upwelling.

2.3. Coral Isotopic Calculation

[14] Modeled surface ocean isotopic ratios are used to calculate coral isotopic ratios in a similar manner to the forward modeling of foraminiferal carbonate isotopic ratios by *Schmidt* [1999b]. We assume that coral isotopic ratios depend only on the local surface ocean isotopic ratio and SST in order to obtain an estimate of the climate-related component of the coral isotope signal. The modeled coral isotopic ratios are also used to validate the modeled surface ocean isotopic ratio, as continuous surface ocean isotopic measurements are not widely available whereas coral $\delta^{18}\text{O}$ records exist for a large number of sites across the tropics [e.g., *Gagan et al.*, 2000].

[15] The model coral $\delta^{18}\text{O}$ is calculated from the prescribed SSTs and modeled $\delta^{18}\text{O}$ values using an empirical relationship derived by *Juillet-Leclerc and Schmidt* [2001]:

$$\delta^{18}\text{O}_{coral} = \delta^{18}\text{O}_{ocean} + a(\text{SST}) + b \quad (3)$$

where SST is given in $^{\circ}\text{C}$, and $a = -0.20 \pm 0.02\text{‰ }^{\circ}\text{C}^{-1}$ and $b = 0.45$ represent typical values for the *Porites* genus of coral which is commonly used for paleoclimate reconstructions. An additional offset of -0.27‰ is needed to convert the $\delta^{18}\text{O}$ values from the VSMOW standard used for precipitation and ocean isotopic ratios to the coral carbonate PDB standard [*Hut*, 1987]. The empirical relationship used here does not differ substantially from those found in other

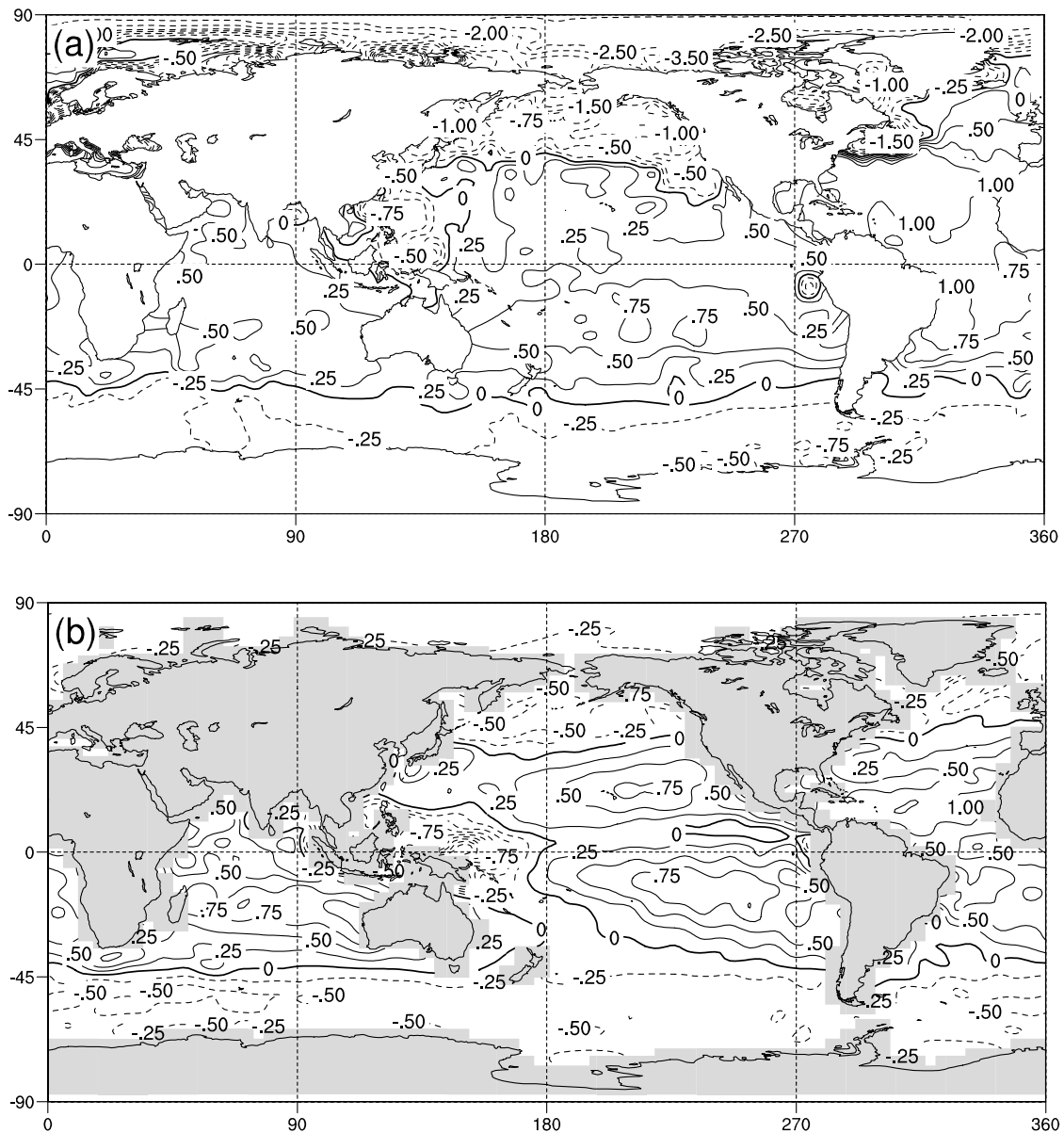


Figure 1. (a) Observed surface ocean $\delta^{18}\text{O}$ from Global Seawater Oxygen-18 Database (with missing values filled) and (b) annual average modeled surface ocean $\delta^{18}\text{O}$. Contour interval is 0.25‰ below $\pm 1\%$ and 0.5‰ otherwise.

studies for *Porites* and other species of reef-building coral [e.g., Wellington *et al.*, 1996].

3. Surface Ocean Climatology

[16] Two climatological model runs were first carried out to test the surface ocean isotopic scheme. The GISST2.3b monthly SST fields [Rayner *et al.*, 1996], averaged from 1980–1999, were used as boundary conditions for the 20-year annually repeating model runs. The surface ocean isotopic ratio was set to a constant value of $R = R_{VSMOW}$ for the first run, and for the second run the interactive surface ocean scheme was used with a mean deep ocean ratio of $R_{deep} = R_{VSMOW}$ and initialized from a constant surface ocean isotopic ratio.

[17] In Figure 1, the annual average modeled surface ocean isotopic distribution is compared with the observed Global Seawater Oxygen-18 Database surface ocean isotopic distribution. The observed distribution consists of measurements from the upper 50 m of the ocean interpolated onto a $4^\circ \times 5^\circ$ grid with missing values filled using an area-weighted interpolation scheme. The large-scale features of the tropical and midlatitude distribution are well reproduced by the model, and the modeled surface ocean $\delta^{18}\text{O}$ values are generally within 0.5‰ of the observed values at these latitudes. The modeled surface ocean $\delta^{18}\text{O}$ distribution closely resembles the mean modeled precipitation minus evaporation distribution (not shown), indicating that variability of the isotopic content of precipitation and evaporation are second-order effects.

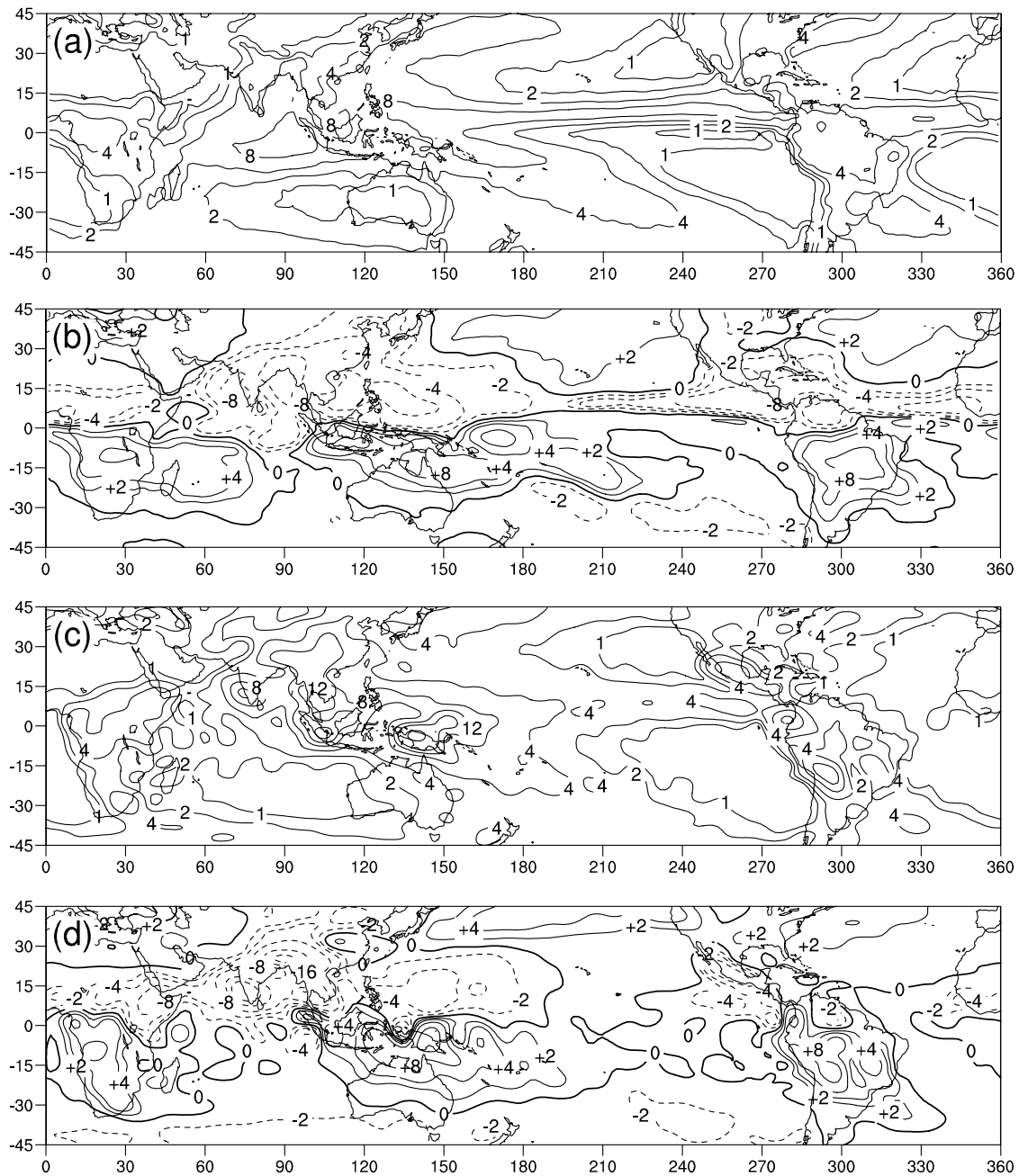


Figure 2. Observed CMAP precipitation: (a) annual average and (b) DJF–JJA and modeled precipitation: (c) annual average and (d) DJF–JJA. Contours are 1, 2, 4, 8, 12, 16, and 24 mm d^{-1} for annual averages and 0, ± 2 , 4, 8, 16, and 24 mm d^{-1} for differences.

[18] The model captures the observed isotopic enrichment due to the local excess of evaporation over precipitation in the subtropical Pacific, Atlantic and Indian Oceans. The relatively depleted surface ocean isotopic ratios in the western Pacific Warm Pool due to the high precipitation in this region are also reproduced. The model does not reproduce the large negative $\delta^{18}\text{O}$ values associated with runoff of isotopically depleted continental precipitation and snowmelt at high northern latitudes for the reasons discussed above. The absence of horizontal transport prevents the scheme from simulating the observed smoothing of surface ocean isotopic gradients due to the transport of

isotopically enriched tropical waters poleward on western boundaries and isotopically depleted waters equatorward along eastern ocean boundaries.

[19] The atmospheric response to variable surface ocean isotopic ratios was also investigated by comparing the modeled isotopic ratios in precipitation and atmospheric water vapor with and without the interactive isotopic surface ocean scheme. The spatial pattern of differences between the two runs is a largely linear response to the surface ocean isotopic forcing (not shown). The near linear response of precipitation isotopic ratios in the tropics to the surface ocean distribution is strong evidence that a large proportion

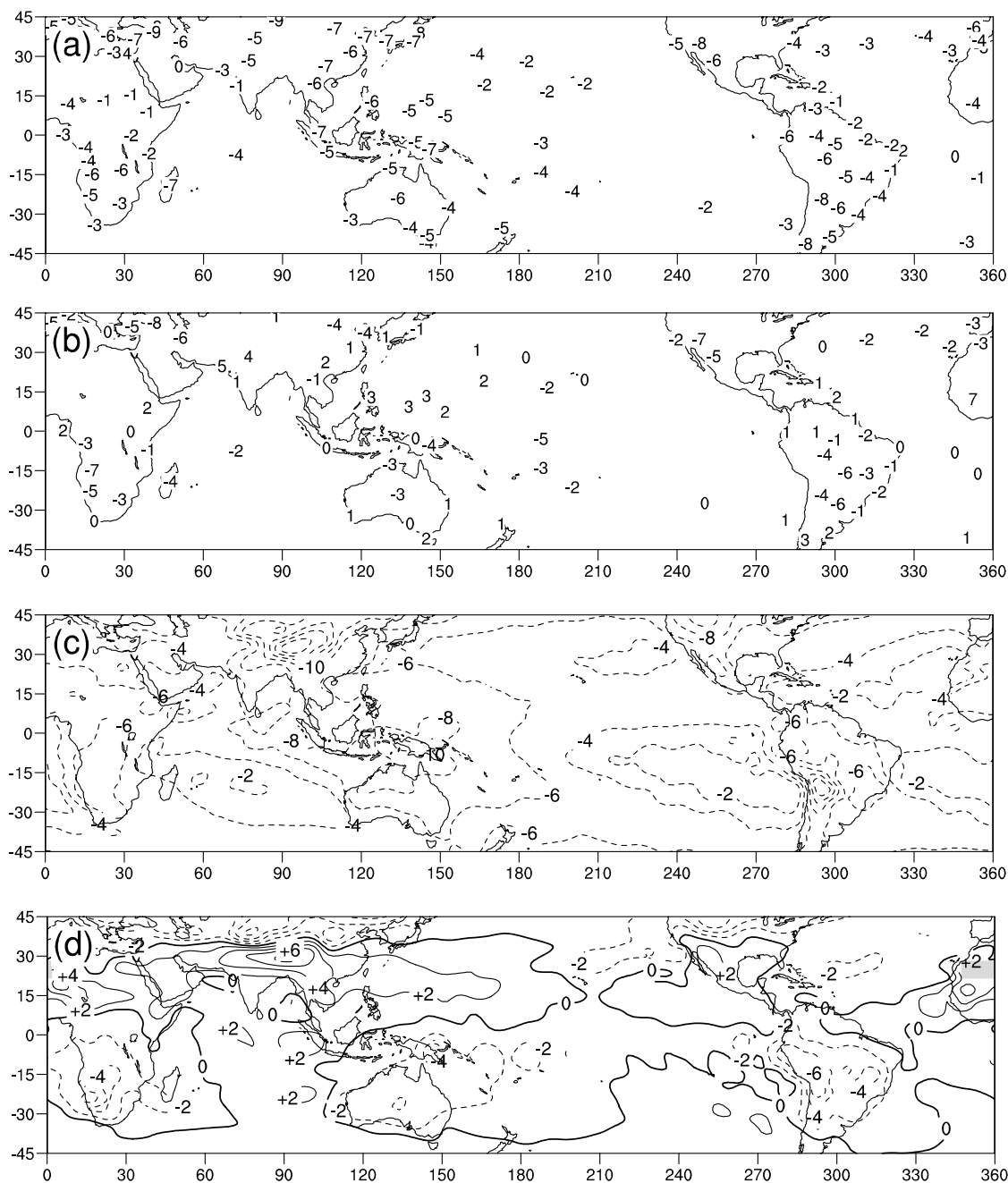


Figure 3. Observed GNIP precipitation $\delta^{18}\text{O}$: (a) annual average and (b) DJF–JJA and modeled precipitation $\delta^{18}\text{O}$: (c) annual average and (d) DJF–JJA. Contour interval is 2‰.

of the moisture source for tropical precipitation is local, in agreement with previous studies [e.g., Cole *et al.*, 1999]. Our results indicate that a constant surface ocean isotopic ratio or mean observed surface ocean isotopic distribution is sufficiently accurate as a boundary condition for atmospheric isotopic tracer models. However, the interactive scheme offers the additional ability to model the temporal variability of surface ocean isotopic ratios.

4. Transient 1950–1999 Simulation

[20] The variability of the isotopic composition of precipitation and surface ocean water on seasonal and interan-

nual timescales is examined for a 50-year climate simulation forced with monthly GISST2.3b SST and sea ice coverage data from 1950–1999 [Rayner *et al.*, 1996]. The SST and sea ice fields were first interpolated onto the MUGCM R21 spectral transform grid and land surface boundary conditions for the model were constructed using constant monthly snow coverage averaged from 1979–1985 observational data from the NIMBUS-7 satellite. Mean ozone concentrations were prescribed from 1970s and 1980s TOMS satellite observations and observed annual average atmospheric carbon dioxide concentrations increasing from 311 ppmv in 1950 to 368 ppmv in 1999 [Schimel *et al.*, 1996; Keeling and Whorf, 2000] were used to construct

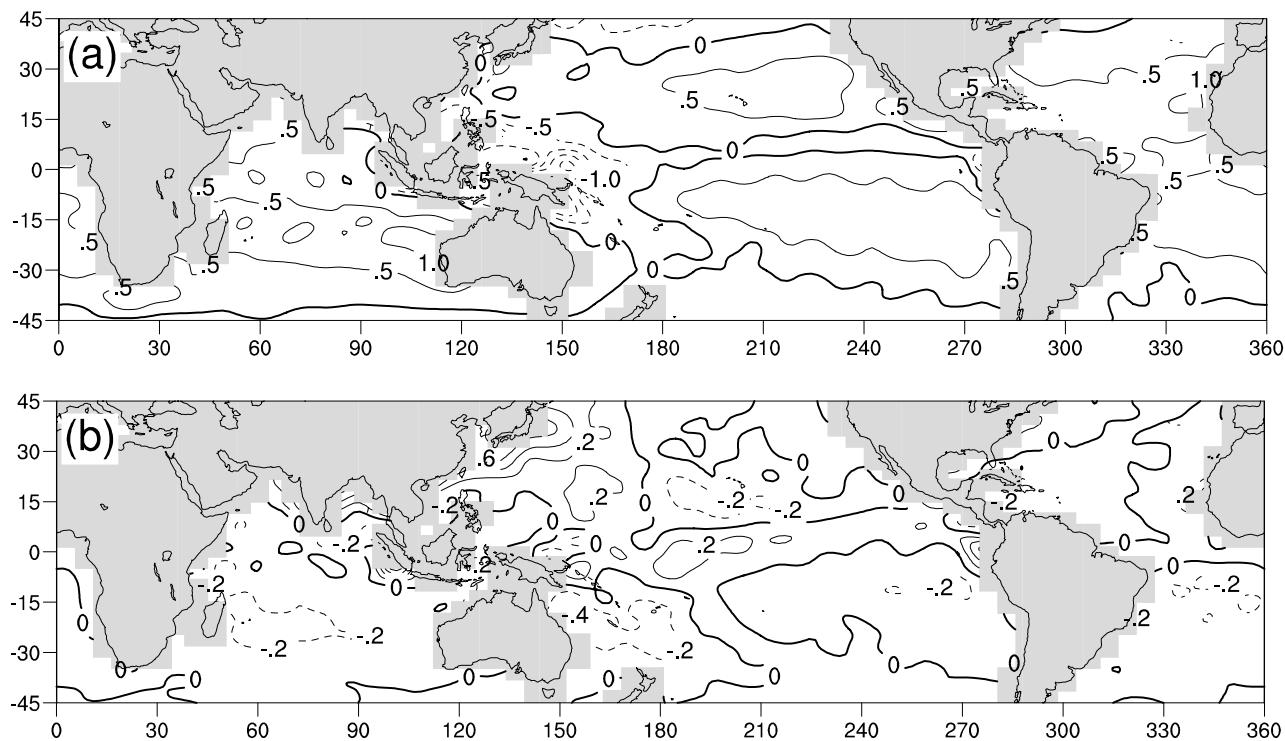


Figure 4. Modeled surface ocean $\delta^{18}\text{O}$: (a) annual average and (b) DJF–JJA. Contour intervals are 0.5‰ and 0.2‰, respectively.

annual radiation transfer coefficients for each year of the simulation. The mean deep ocean isotopic ratio was set to $R_{\text{deep}} = R_{\text{VSMOW}}$. The model was initialized from a climatological state with isotopic ratios set to R_{VSMOW} and boundary conditions for 1945–1949 were used to spin-up the model for five years prior to the 50-year simulation.

4.1. Tropical Seasonal Cycle

[21] The isotopic response to the seasonal variability of precipitation, temperature and atmospheric circulation in the tropics is investigated for the 50-year transient simulation. Seasonal and interannual monsoon signals have been identified in isotope records from Tibetan Plateau ice cores [e.g., Thompson, 2000] and corals in the western Pacific and Indian Oceans [e.g., Charles *et al.*, 2003] suggesting that isotope records may be used to investigate variability of monsoon strength and teleconnections. If the model is able to simulate the tropical climate and isotopic seasonality correctly, it may be more confidently used in the interpretation of such isotope records.

[22] The MUGCM seasonal precipitation cycle is compared with observed monthly CPC Merged Analysis of Precipitation (CMAP) precipitation data from 1979–2000 [Xie and Arkin, 1996]. The observed and modeled precipitation for the austral summer (December–January–February, DJF) and boreal summer (June–July–August, JJA) are shown in Figure 2. The MUGCM is able to simulate the main features of the seasonal precipitation distribution in the tropics as well as other atmospheric models of comparable resolution [e.g., Gates *et al.*, 1999]. One of main shortcomings of the modeled precipitation distribution is the simulation of excessive precipitation

over elevated topography, which is a well known limitation of the convection scheme of Manabe *et al.* [1965]. The seasonal migration of the tropical convergence zones is generally well reproduced, although the precipitation distribution associated with the ITCZ is not well resolved in the central and eastern equatorial Pacific or the tropical Atlantic, leading to a poor representation of the seasonal cycle in this region. As the topography of the Himalayas is not fully resolved in the model, the Asian summer monsoon extends slightly further north than observed, with the maximum northward extent of modeled monsoon precipitation between 35°N and 40°N.

[23] The modeled precipitation isotopic ratios are compared with records from the GNIP database, as shown in Figure 3. In order to compare the GNIP data with seasonal averages from the model, precipitation-weighted means are calculated for all stations with more than 36 months of data. While this leads to a small sample size for some stations, it was desirable to include tropical island stations with relatively short records, and the results were found to be largely insensitive to the choice of threshold [Brown, 2004]. Because of the high density of stations in some regions, averages are shown for those areas with more than one station within a 500 km radius. The model reproduces the observed GNIP seasonality of isotopes in precipitation within 1–2‰ for most tropical sites, in agreement with the study of Noone and Simmonds [2002] using the previous version of the MUGCM. The inclusion of variable surface ocean isotopic ratios improves the representation of the atmospheric isotopic composition in some regions. However, the surface ocean isotopic distribution is influenced by many of the same model biases as the precipitation

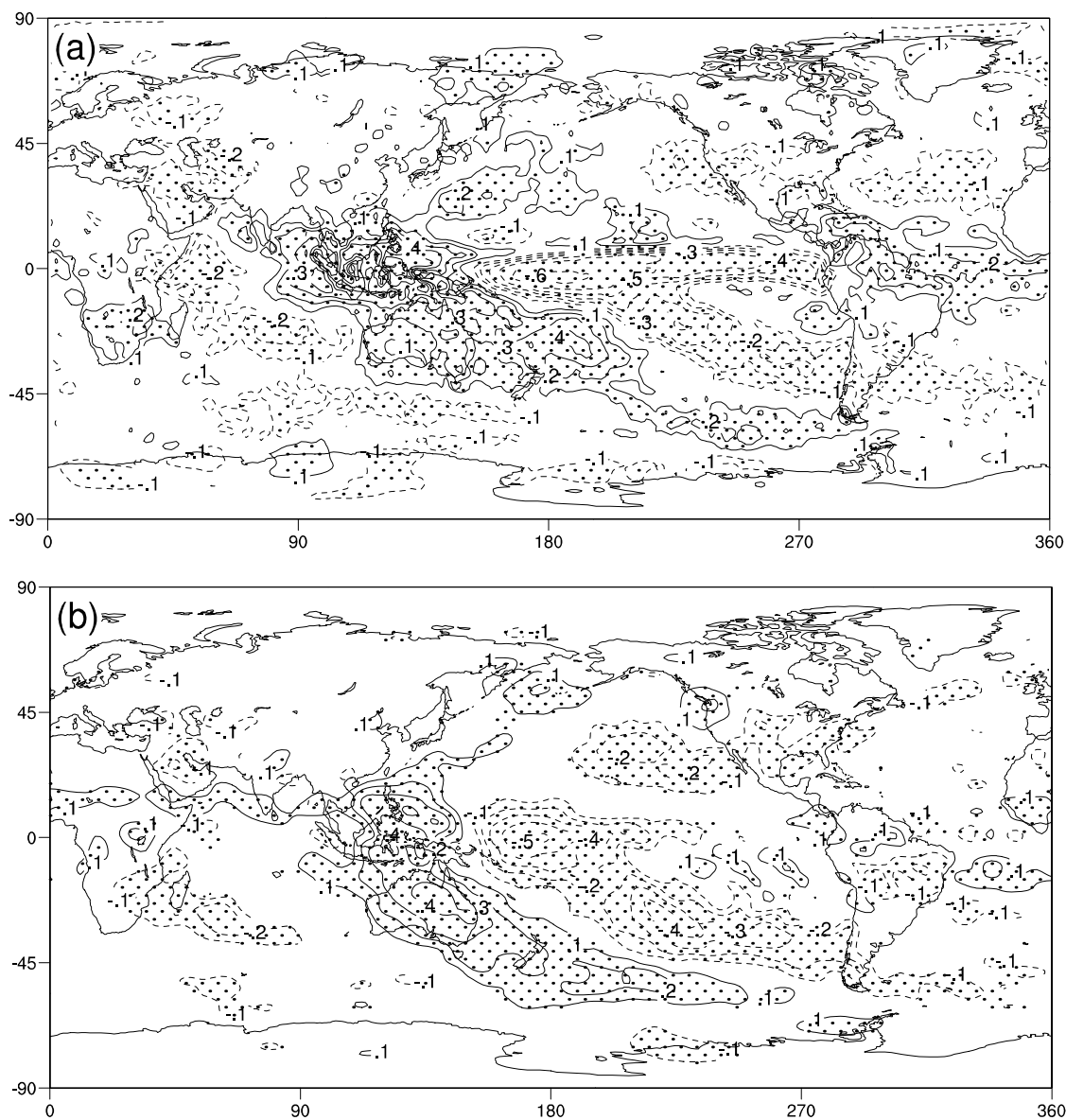


Figure 5. Correlation between (a) monthly anomalies of observed CMAP precipitation and SOI and (b) monthly anomalies of modeled precipitation and SOI. Contour interval is 0.1; zero contour is not shown. Stippled regions are significant correlations at 95% confidence level.

isotope signal (e.g., errors in precipitation amount), leading to greater biases in some regions.

[24] Comparison with Figure 2 indicates that a large component of the simulated seasonal isotope signal in the tropics is associated with changes in precipitation amount. The seasonal meridional migration of the ITCZ is seen in the changing location of the region of most negative precipitation $\delta^{18}\text{O}$ values. Seasonal isotopic depletion is also seen during the peak of the Asian, West African, South American and Australian summer monsoons. In the midlatitudes, the influence of seasonal temperature variability competes with precipitation amount, with the approximate limit of the dominant precipitation amount influence at the poleward extent of the monsoonal flow and the ITCZ [Araguas-Araguas *et al.*, 1998].

[25] The seasonal cycle of modeled surface ocean isotopic ratios is shown in Figure 4. Comparison with Figure 2

indicates that the modeled surface ocean isotopic ratios in the tropics are strongly influenced by the seasonal variation of precipitation. The largest modeled seasonal isotopic ranges of around 1‰ are seen in the tropical Indian and western Pacific Oceans. In the southern Indian Ocean, the greatest isotopic depletion occurs in DJF, while isotopic depletion in the Arabian Sea and Bay of Bengal is greatest in JJA in agreement with observations [Delaygue *et al.*, 2001]. The Australian summer monsoon coincides with increased surface ocean isotopic depletion in the southwestern Pacific, while surface ocean $\delta^{18}\text{O}$ values are most depleted in JJA in the northwestern Pacific. The magnitude of the modeled surface ocean isotopic seasonal cycle is not compared with observations as only a small number of seasonal measurements of seawater $\delta^{18}\text{O}$ in the upper 50 m of the ocean are available from the Global Seawater Oxygen-18 Database database, and a number of these sites

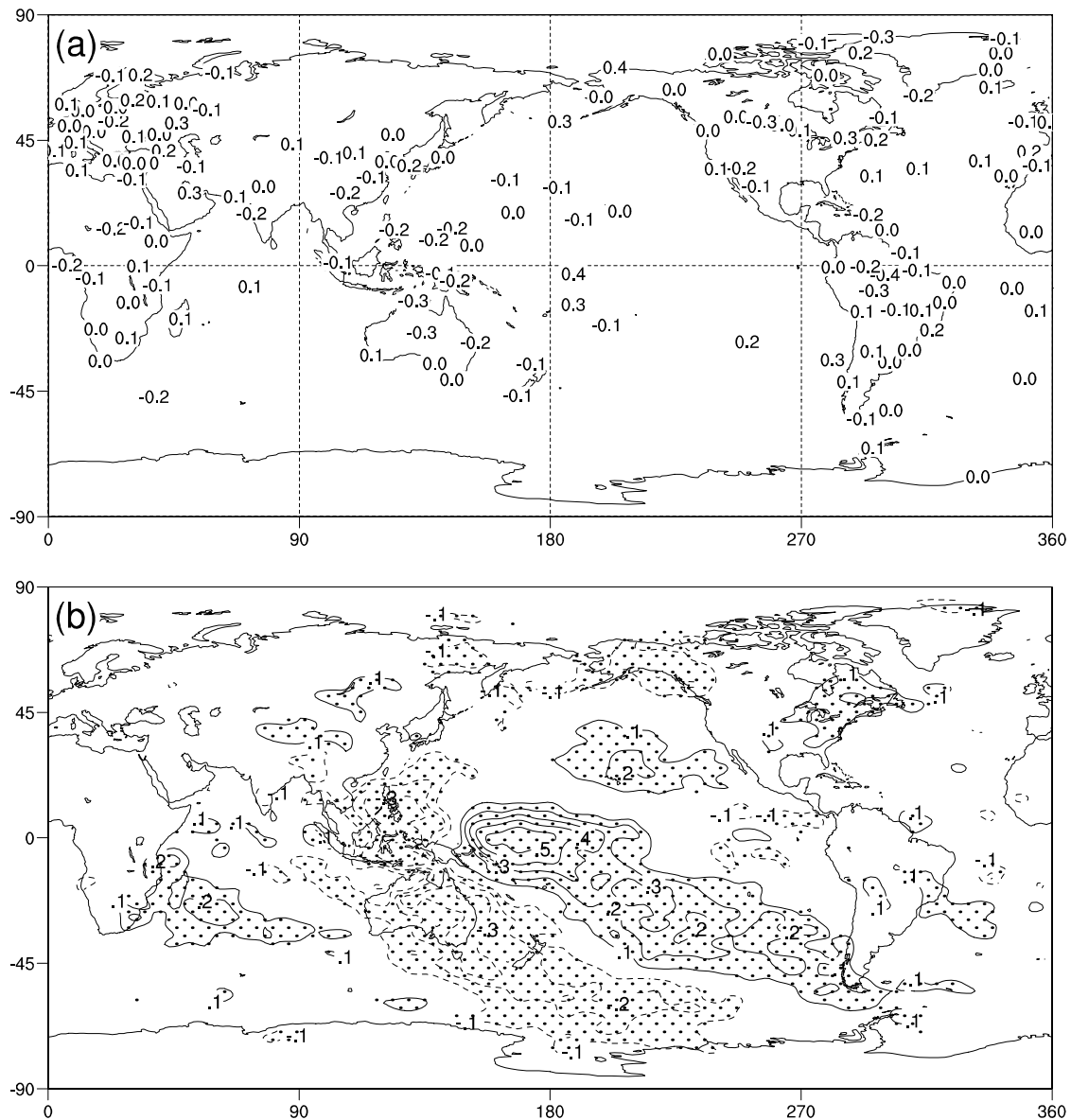


Figure 6. Correlation between (a) monthly anomalies of observed GNIP precipitation $\delta^{18}\text{O}$ and SOI and (b) monthly anomalies of modeled precipitation $\delta^{18}\text{O}$ and SOI. Contour interval is 0.1 for Figure 6b; zero contour is not shown. Stippled regions are significant correlations at 95% confidence level.

are estuaries or lagoons where local conditions are unlikely to represent the large-scale open ocean conditions simulated by the model.

4.2. ENSO

[26] ENSO is the strongest mode of interannual variability in the tropics, producing variability in precipitation, temperature and atmospheric circulation, all of which influence the isotopic ratio of precipitation. Changes in SSTs and local hydrology as well as upwelling and ocean advection associated with ENSO may alter the surface ocean isotopic ratio. ENSO signals have been identified in coral isotope records [e.g., *Tudhope et al.*, 2001; *Cobb et al.*, 2003] and in tropical ice core records [e.g., *Bradley et al.*, 2003; *Hoffmann et al.*, 2003]. We examine the modeled response of isotopic ratios of precipitation and the surface ocean to

ENSO and compare this response with observations and previous studies.

[27] The observed association between precipitation and ENSO is identified using the correlation between observed CMAP precipitation data for the period 1979–2000 and the Southern Oscillation Index (SOI) of ENSO strength from the Australian Bureau of Meteorology. The observed association is compared with the correlation between modeled precipitation and SOI (calculated from the simulated mean sea level pressure interpolated to the locations of Darwin and Tahiti), as shown in Figure 5. The model reproduces many features of the observed precipitation response to ENSO with negative correlations in the central Pacific and positive correlations over the western Pacific Warm Pool and South Pacific Convergence Zone resulting from a shift in the location of the

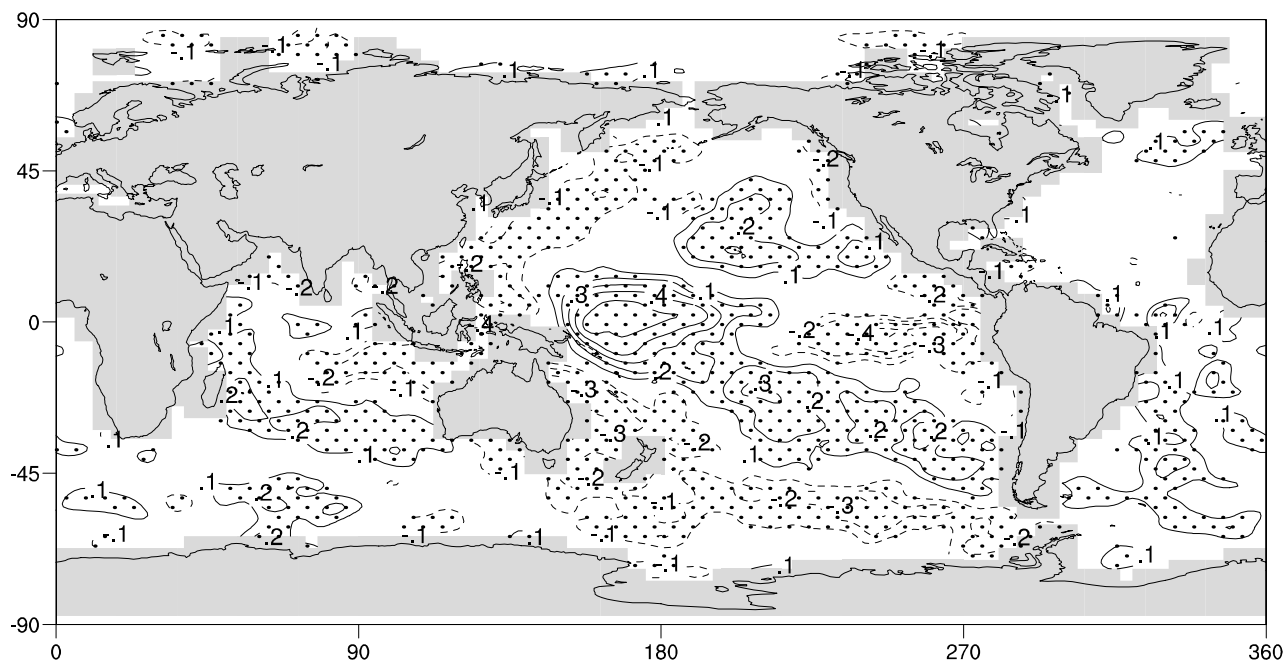


Figure 7. Correlation between monthly anomalies of modeled surface ocean $\delta^{18}\text{O}$ and SOI. Contour interval is 0.1 and zero contour is not shown. Stippled regions are significant correlations at 95% confidence level.

Walker circulation during El Niño events. However, the modeled negative correlations, indicating increased precipitation during El Niño events, do not extend into the eastern Pacific as observed. Over the equatorial Atlantic and tropical South America, the model does not simulate the decrease in precipitation during El Niño events seen in observations.

[28] The response of modeled precipitation isotopic ratios to ENSO is compared with the ENSO signal in observed GNIP station records. The correlations between modeled and observed precipitation $\delta^{18}\text{O}$ and SOI are shown in Figure 6, with stippling indicating correlations which are significant at the 95% confidence level according to a Student's t test. The precipitation-weighted monthly $\delta^{18}\text{O}$ anomalies from all GNIP stations with more than 36 months of data are correlated with the observed monthly SOI values for the same months. The observed $\delta^{18}\text{O}$ -SOI correlations are averaged as before over regions with a high density of stations. As some of the GNIP records are discontinuous and cover different subperiods within the modeled period, the observed correlations are not precisely comparable with the modeled correlations.

[29] Large positive $\delta^{18}\text{O}$ -SOI correlations are simulated in the central equatorial Pacific where the model reproduces the observed precipitation response to El Niño and La Niña events, in agreement with the previous isotopic modeling studies of *Hoffmann et al.* [1998] and *Cole et al.* [1999]. Negative correlations over the western tropical and subtropical Pacific in the observations are also reproduced by the model. Strong negative correlations over tropical South America in the observations are not reproduced by the model, which is consistent with the weak modeled precipitation response to ENSO in this region. Significant correlations extend via atmospheric teleconnec-

tions from the tropical central and western Pacific to high Southern latitudes.

[30] Surface ocean $\delta^{18}\text{O}$ also responds to changes in precipitation and evaporation associated with ENSO. The modeled correlation between surface ocean $\delta^{18}\text{O}$ and SOI is shown in Figure 7, while the observed ENSO signal in selected coral $\delta^{18}\text{O}$ records is compared with the modeled response in section 6. The correlation between modeled $\delta^{18}\text{O}$ and SOI is strongly positive in the central Pacific in the region of enhanced precipitation during El Niño events, with positive correlations extending to the midlatitudes in the eastern Pacific. Over the far western Pacific and Indian Ocean, negative correlations indicate reduced precipitation and reduced isotopic depletion during El Niño events. In the eastern Pacific Ocean, warmer SSTs during El Niño events lead to increased evaporation and relatively enriched surface ocean $\delta^{18}\text{O}$ values producing a negative correlation between ocean $\delta^{18}\text{O}$ and SOI in this region. As the scheme does not include horizontal advection, it does not capture the observed zonal displacement of the Warm Pool and associated anomalous zonal advection during ENSO events which alters the salinity distribution in the equatorial Pacific [*Picaut et al.*, 1996], and would also be expected to influence the isotopic distribution.

5. Ice Core Records

[31] Modeled precipitation isotopic ratios are compared quantitatively with annually resolved modern ice core isotope records from the South American Andes which cover some or all of the modeled period of 1950–1999, available from the World Data Center for Paleoclimatology (www.ncdc.noaa.gov/paleo). A comparison between modeled isotopic ratios and modeled climate parameters is also

Table 1. Correlations Between Precipitation-Weighted ONDJFMA Average Modeled Precipitation $\delta^{18}\text{O}$ at Andean Ice Core Sites and Selected Climate Parameters

	Surface Temperature	Precipitation Amount	$P - E$ Over Amazon Basin ^a	SOI	Multiple r^b
Huascarán	+0.45 ^c	-0.30 ^c	-0.29 ^c	-0.14	0.64
Quelccaya	+0.42 ^c	-0.64 ^c	-0.30 ^c	-0.22	0.70

^aPrecipitation minus evaporation averaged over $0^\circ - 10^\circ\text{S}$, $280^\circ\text{E} - 325^\circ\text{E}$.

^bMultiple linear regression involving all variables with significant correlations.

^cCorrelations significant at 95% confidence level.

carried out for selected sites on the Tibetan Plateau where ice cores have been retrieved. We investigate how accurately the model is able to reproduce observed ice core isotope records, and examine the regional-scale climate controls on modeled precipitation $\delta^{18}\text{O}$ at each of the ice core sites.

5.1. South American Andes

[32] The modeled precipitation $\delta^{18}\text{O}$ is compared with two modern ice core records from Huascarán ($9^\circ 06'\text{S}$, $77^\circ 30'\text{W}$) and a single record from Quelccaya ($13^\circ 56'\text{S}$, $70^\circ 50'\text{W}$) in the tropical Andes [Thompson *et al.*, 1985, 1995]. Previous studies have put forward several mechanisms to explain the seasonal isotopic cycle in precipitation over the Andes. Grootes *et al.* [1989] argue that the Andean $\delta^{18}\text{O}$ is controlled by changes in the rainout of Atlantic moisture during transport over the Amazon basin, with greater rainout and isotopic depletion during the summer wet season. Thompson *et al.* [2000a] propose that isotopic depletion is associated with the seasonal shift to a higher condensation height (with cooler condensation temperatures) during summer convective thunderstorms over the Andes. In addition, recent modeling studies suggest that interannual variability of Andean isotopic ratios is influenced by ENSO via changes in the amount of precipitation over the Amazon basin [Hoffmann *et al.*, 2003; Vuille *et al.*, 2003a] and changes in accumulation rates and freezing levels over the Andes [Bradley *et al.*, 2003].

[33] The modeled precipitation $\delta^{18}\text{O}$ is interpolated to the locations of the ice core sites. The modeled isotopic values at both sites are less depleted than the observed ice core values, consistent with the lower Andean topography in the model (1488 m at Huascarán compared with the real height of 6050 m, 2757 m at Quelccaya compared with 5670 m). The controls on the interannual variability of modeled precipitation $\delta^{18}\text{O}$ at the ice core sites are investigated via correlations between precipitation-weighted averages of $\delta^{18}\text{O}$ and local temperature and precipitation, precipitation minus evaporation over the Amazon basin and modeled SOI, shown in Table 1. The averages are calculated for the wet season months of October–April (ONDJFMA), following the approach of Vuille *et al.* [2003b], with dependent and independent variables weighted by the local monthly precipitation amount.

[34] The model simulates a significant positive correlation between $\delta^{18}\text{O}$ and local temperature and significant negative correlation between $\delta^{18}\text{O}$ and local precipitation at both core sites, in agreement with the results of Vuille *et al.* [2003b]. The modeled precipitation isotopic ratios at both sites are also significantly correlated with precipitation

minus evaporation over the Amazon basin, indicating the importance of isotopic rainout over the basin during moisture transport. The correlation with SOI is not significant for either core site, which reflects the weak ENSO signal in precipitation simulated over tropical South America. A multiple linear regression is carried out for those variables which are significantly correlated with the modeled precipitation isotopic ratios, as shown in Table 1, resulting in a stronger correlation than for any individual variable in each case.

[35] The modeled precipitation $\delta^{18}\text{O}$ interpolated to the core sites is not significantly correlated with ice core $\delta^{18}\text{O}$ from the two Huascarán cores ($r < 0.1$ for both cores), while modeled $\delta^{18}\text{O}$ is significantly correlated at the 94% level with the Quelccaya ice core $\delta^{18}\text{O}$ record although with only a modest correlation strength ($r = 0.32$). We also note that interannual and decadal variability in the ice core records is not significantly correlated with modeled isotopic ratios of water vapor at 500 hPa over the Amazon basin. This is in contrast with the strong relationship identified by Hoffmann *et al.* [2003] between the AII (mean of four Andean ice core records from 1909–1998) and modeled Amazon basin water vapor isotopic content from the ECHAM model.

[36] It appears that the model does not fully capture the interannual variability of precipitation associated with ENSO over the tropical Andes, which has been found to influence the Huascarán and Quelccaya isotope records [e.g., Hoffmann *et al.*, 2003; Bradley *et al.*, 2003]. One likely reason for the poor simulation of ENSO precipitation teleconnections over the region is the lower resolution of Andean topography in MUGCM compared with the models used in the study of Vuille *et al.* [2003b]. The resolution of Andean topography in climate models may limit the simulation of atmospheric blocking and the relative contributions of Pacific and Atlantic moisture to Andean precipitation [Valdes, 2000]. The limitations of the model convection scheme over elevated topography may also be a factor in the inability of the model to reproduce observed isotopic variability in this region.

5.2. Tibetan Plateau

[37] The relationship of modeled precipitation $\delta^{18}\text{O}$ with various climate parameters is also considered at locations corresponding to the Dunde [Thompson *et al.*, 1989], Guliya [Thompson *et al.*, 1997] and Dasuopu [Thompson *et al.*, 2000b] ice core sites. The modeled relationships are compared with climate-isotope relationships suggested for Tibetan Plateau ice core records in previous studies [e.g., Thompson, 2000; Bradley *et al.*, 2003]. The influence of the Asian monsoon and ENSO on the modeled isotope signal is also investigated. The All India Rainfall (AIR) index, which is the sum of precipitation over the Indian continent for the months June–September (JJAS), is used to quantify the intensity of the South Asian monsoon. While other indices may capture large-scale monsoon circulation more reliably (e.g., indices based on wind shear), AIR is an appropriate index for considering the impact of monsoon precipitation amount on atmospheric moisture isotopic content. Similar results are obtained when a dynamical monsoon index is used [Brown, 2004].

[38] The Dunde ice core site ($38^\circ 06'\text{N}$, $96^\circ 25'\text{E}$) is on the northeast Tibetan Plateau while the Guliya ice core site

Table 2. Correlations Between Precipitation-Weighted JJAS Average Modeled Precipitation $\delta^{18}\text{O}$ at Tibetan Plateau Ice Core Sites and Selected Climate Parameters

	Surface Temperature	Precipitation Amount	Northern Hemisphere Temperature ^a	AIR	SOI	Multiple r^b
Guliya	-0.46 ^c	-0.52 ^c	+0.01	-0.15	-0.12	0.65
Dunde	+0.17	-0.58 ^c	+0.10	-0.09	-0.04	-
Dasuopu	+0.19	-0.53 ^c	+0.24	-0.46 ^c	-0.45 ^c	0.63

^aAverage Northern Hemisphere surface temperature.

^bMultiple linear regression involving all variables with significant correlations.

^cCorrelations significant at 95% confidence level.

(35°17'N, 81°29'E) is on the northwest of the Plateau. On the northern Tibetan Plateau, precipitation $\delta^{18}\text{O}$ is observed to vary with temperature over the seasonal cycle [Yao *et al.*, 1996]. The Dasuopu site (28°23'N, 85°43'E) lies on the southern Tibetan Plateau within the direct influence of the south Asian monsoon where the most isotopically depleted precipitation occurs during the summer wet season [Thompson *et al.*, 2000b]. Using summer precipitation samples, Tian *et al.* [2001] confirm that the isotopic composition of precipitation on the northern Tibetan Plateau reflects temperature, while on the southern Tibetan Plateau the greatest influence on precipitation isotopic ratios is precipitation amount due to heavy monsoon rains. Thompson *et al.* [2000b] find that five-year averages of ice core $\delta^{18}\text{O}$ from both Dunde and Dasuopu are more strongly correlated with Northern Hemisphere temperature than local accumulation, arguing for a dominant temperature signal in Tibetan Plateau ice core isotope records.

[39] The precipitation-weighted model average $\delta^{18}\text{O}$ is calculated using values interpolated to the ice core sites for the monsoon season (JJAS), following the approach of Bradley *et al.* [2003]. The modeled isotopic values are compared with precipitation-weighted averages of local temperature, precipitation, average Northern Hemisphere temperature and SOI for the same months. Unweighted AIR values are used as the index is calculated for the summer monsoon months by definition. As shown in Table 2, modeled $\delta^{18}\text{O}$ values are significantly correlated with local precipitation amount at Dunde and Guliya core sites. At Guliya, $\delta^{18}\text{O}$ is significantly negatively correlated with local temperature, suggesting an indirect relationship with temperature via monsoon strength or precipitation amount. Modeled $\delta^{18}\text{O}$ at Dasuopu is strongly correlated with local precipitation amount, AIR index and SOI, indicating an ENSO influence on Tibetan Plateau moisture and isotopic depletion in agreement with the study of Bradley *et al.* [2003]. Multiple linear regressions are calculated for Guliya and Dasuopu using all variables with significant correlations with $\delta^{18}\text{O}$, as shown in Table 2. Partial correlations of local precipitation, AIR and SOI with modeled $\delta^{18}\text{O}$ at Dasuopu are reduced for precipitation amount ($r = -0.18$) and for AIR ($r = -0.23$) but almost unchanged for SOI ($r = -0.39$), suggesting that local precipitation amount and monsoon strength are related while ENSO influence is largely independent of these other variables.

[40] The lack of significant positive correlations with local temperature and Northern Hemisphere temperature is in disagreement with the interpretation of these records as temperature proxies [e.g., Yao *et al.*, 1996; Thompson *et al.*, 2000b]. While temperature influences on precipitation

$\delta^{18}\text{O}$ may be more important on longer timescales not investigated here, it may also be the case that the model overestimates the precipitation amount effect for the northern Tibetan Plateau sites. As discussed in section 4.1, the low resolution of Himalayan topography in the model permits monsoon moisture to penetrate too far inland. This results in excessive precipitation over the northern Tibetan Plateau and a precipitation amount control over the extent of isotopic depletion, in contrast with the observed dry conditions and temperature control over isotopic ratios of precipitation [e.g., Tian *et al.*, 2001]. The lack of a prognostic snow scheme with isotopic tracers may also limit the accuracy of the simulation in this region both due to the lack of local and large-scale climate feedbacks with variable snow coverage, and the role of snowmelt in continental moisture recycling.

6. Coral Records

[41] Coral oxygen isotope records from Mahe Island in the Indian Ocean [Charles *et al.*, 1997], Madang in the western Pacific [Tudhope *et al.*, 2001] and Maiana Island in the central Pacific [Urban *et al.*, 2000] are compared with modeled coral isotopic ratios calculated from surface ocean isotopic ratios and SST using the method described in section 2. Coral records were chosen which covered at least 40 years of the period 1950–1999 for a range of tropical sites from the World Data Center for Paleoclimatology. While the coral records have subannual sampling resolution, annual average isotopic ratios are considered here to highlight interannual variability.

[42] At Mahe Island, Republic of the Seychelles, in the southwestern Indian Ocean, the observed seasonal cycle of coral $\delta^{18}\text{O}$ is controlled by SST variability, while the interannual coral isotope signal also follows SST, which is influenced by both ENSO and monsoon variability [Charles *et al.*, 1997]. At Madang, Papua New Guinea, in the western Pacific Warm Pool, coral $\delta^{18}\text{O}$ has a dependence on both SST and precipitation variability, with a stronger precipitation influence on interannual timescales [Tudhope *et al.*, 1995]. The combined influence of SST and precipitation variability produces a strong interannual ENSO signal in coral isotopic ratios from this site, with decreased (increased) precipitation and cooler (warmer) SSTs during El Niño (La Niña) events, allowing the reconstruction of paleo-ENSO records from fossil corals [Tudhope *et al.*, 2001]. At Maiana Island, Republic of Kiribati, in the central equatorial Pacific, coral isotopic ratios are primarily controlled by variability in surface ocean $\delta^{18}\text{O}$ associated with precipitation amount [Urban *et al.*, 2000]. On interannual timescales, precipitation variability associated with ENSO therefore

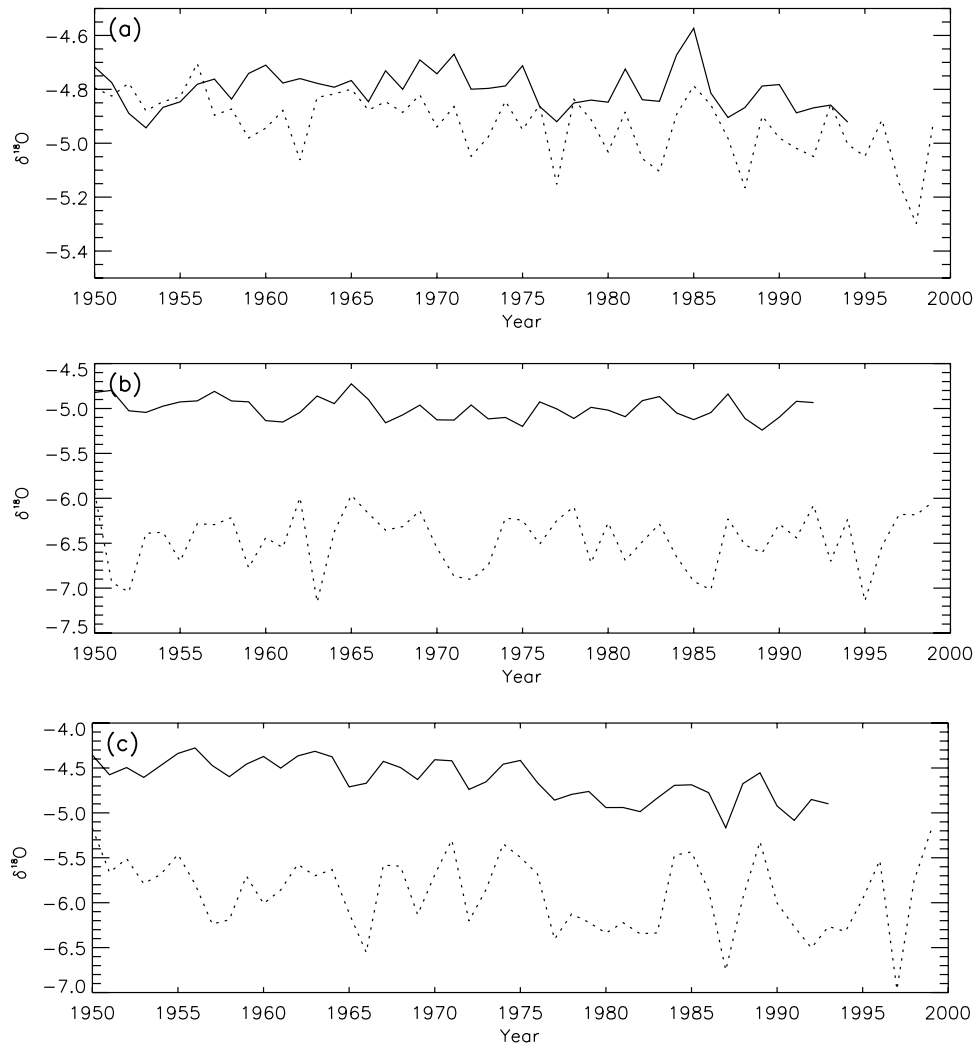


Figure 8. Annual average observed (solid line) and modeled (dotted line) coral $\delta^{18}\text{O}$ from (a) Mahe Island, Indian Ocean, (b) Madang, western Pacific, and (c) Maiana Island, central Pacific.

results in a strong ENSO signal in the Maiana coral oxygen isotope record.

[43] The annual average observed and modeled coral $\delta^{18}\text{O}$ values for the three sites are shown in Figure 8 and the correlations between modeled and observed coral $\delta^{18}\text{O}$ and SOI are given in Table 3. The significance of the correlations is assessed taking into consideration the autocorrelation in the time series by adjusting the degrees of freedom [von Storch and Zwiers, 1999].

[44] The interannual variability of modeled coral isotopic ratios at Mahe Island is dominated by surface ocean $\delta^{18}\text{O}$ variability rather than SST. The mean modeled coral $\delta^{18}\text{O}$ is within 0.1‰ of the observed value, while the variability of the modeled time series is slightly larger (standard deviation, σ , of 0.12‰) than observed ($\sigma \simeq 0.08‰$).

As modeled interannual precipitation variability at this site is less strongly correlated with ENSO than observed precipitation (see Figure 5), the correlation between the modeled coral $\delta^{18}\text{O}$ and SOI is lower than for the observed records. The modeled and observed coral isotopic ratios are significantly correlated, but the model captures less than 20% of the observed variance. For the period of the simulation both modeled and observed annual average coral $\delta^{18}\text{O}$ show no significant correlation with Asian monsoon strength as measured by the AIR monsoon index.

[45] The modeled coral isotopic ratio at Madang is around 1.5‰ more depleted than observed because of the high precipitation simulated at this site, and the modeled coral

Table 3. Correlations Between Modeled and Observed Coral Isotopic Ratios and SOI

Coral Site	Location	Period of Record	$\delta^{18}\text{O}_{obs}$	$\delta^{18}\text{O}_{model}$	$\delta^{18}\text{O}_{obs}$
			Versus $\delta^{18}\text{O}_{model}$	Versus SOI	Versus SOI
Mahe Island	4°S, 55°E	1950–1995	+0.35 ^a	+0.29 ^a	+0.49 ^a
Madang	5°S, 145°E	1950–1992	+0.17	−0.05	−0.43 ^a
Maiana Island	1°N, 173°E	1950–1993	+0.73 ^a	+0.83 ^a	+0.73 ^a

^aCorrelations significant at 95% confidence level.

isotopic variability is around three times larger than observed, reflecting the high interannual precipitation variability simulated by the model at this site ($\sigma \approx 20$ mm/day, compared with $\sigma \approx 8$ mm/day for CMAP observed precipitation). The modeled coral isotopic ratio is not significantly correlated with the observed record at this site as the model does not correctly simulate the strong precipitation and surface ocean $\delta^{18}\text{O}$ response to ENSO which dominates the observed coral signal at Madang. The weak ENSO signal in the model is due to the location of the site at the western edge of the central Pacific ENSO precipitation anomaly, which extends too far west in the model as seen in Figure 6. The weak correlation between modeled and observed annual coral $\delta^{18}\text{O}$ may also be due to the importance of factors such as ENSO-related advection and upwelling which are omitted in the model.

[46] At Maiana Island in the central Pacific, the strong observed ENSO precipitation signal is well reproduced by the model. As the surface ocean and coral isotopic ratios at this site are largely controlled by precipitation variability, this results in a strong correlation between modeled and observed interannual coral $\delta^{18}\text{O}$ variability. The modeled coral isotopic ratio is therefore strongly correlated with SOI at Maiana Island, in agreement with the observed correlation. The model overestimates precipitation at this location, resulting in a mean modeled coral $\delta^{18}\text{O}$ which is around 1.5‰ more depleted than observed. The modeled interannual coral $\delta^{18}\text{O}$ range is almost twice as large as the observed range, although precipitation variability is of the observed magnitude, suggesting that the surface ocean isotopic scheme does not fully capture the effects of horizontal and vertical mixing in the central equatorial Pacific. Both observed and modeled Maiana coral isotopic ratios exhibit a statistically significant trend over the period considered. The trend in the observed record is calculated to be -0.013‰ per year over 1950–1993, while the modeled trend is -0.008‰ per year over the 50-year simulation, consistent with a trend toward warmer SSTs and increased precipitation in the central Pacific.

7. Discussion and Conclusions

[47] The simple one-dimensional representation of the surface ocean isotopic budget presented in this study is able to reproduce key features of tropical seasonal and interannual surface ocean isotopic variability within the limitations of the model's simulation of precipitation. The scheme simulates the observed regions of negative surface ocean $\delta^{18}\text{O}$ in the western Pacific and regions of positive surface ocean $\delta^{18}\text{O}$ in the subtropics. A statistically significant surface ocean $\delta^{18}\text{O}$ signal is simulated in the central and western Pacific in response to ENSO precipitation anomalies. The one-dimensional surface ocean isotopic scheme is only able to quantify changes in the component of the surface ocean isotopic distribution controlled by precipitation and evaporation. To simulate surface ocean isotopic ratios in coastal areas and at high latitudes a river runoff scheme would be required, while representation of horizontal transport and vertical mixing is needed if the scheme is to capture the influence of ocean currents and upwelling. If the model is to be used to simulate paleoclimate, such modifications may be necessary to represent

changes in the volume and isotopic content of continental runoff as well as changes in ocean currents and upwelling.

[48] In the 50-year transient climate simulation, the modeled isotopic ratios of tropical precipitation are more closely associated with precipitation amount than temperature on both seasonal and interannual timescales, in general agreement with previous modeling and observational studies. The model has some difficulty reproducing aspects of the mean distribution and seasonal cycle of tropical precipitation, although we note that simulating tropical precipitation accurately remains a challenge for many atmospheric GCMs. Despite these limitations, the model simulates a strong isotopic response to the seasonal Asian, West African, South American and Australian monsoons. The model also simulates a significant isotopic response to ENSO precipitation anomalies in the central and western tropical Pacific, in agreement with observations and previous modeling studies, although the observed ENSO signal in precipitation and $\delta^{18}\text{O}$ over tropical South America is not well reproduced.

[49] The model captures the relationship of precipitation $\delta^{18}\text{O}$ over the Andes with local temperature, precipitation and with precipitation minus evaporation over the Amazon, but does not simulate a strong response to ENSO. This study and others [Valdes, 2000; Vuille *et al.*, 2003a, 2003b] suggest that high-resolution topography is necessary to reproduce the correct atmospheric circulation and moisture transport in this region. The model simulates the influence of precipitation amount, monsoon strength and ENSO over precipitation $\delta^{18}\text{O}$ at Dasuopu on the southern Tibetan Plateau. At Guliya and Dunde on the northern Tibetan Plateau, the model simulates a stronger precipitation amount control than temperature control over precipitation isotopic ratios (with a negative temperature-isotope relationship at Guliya). This result may be biased by the low resolution of the Himalayas in the model, allowing moist oceanic air masses to be transported too far inland and producing convective precipitation with a dominant precipitation amount effect for isotopic ratios at Guliya and Dunde. The ability of the model to simulate isotopic ratios of precipitation at high-altitude ice core sites appears to be limited, although the model would be expected to perform significantly better with higher-resolution topography.

[50] The application of a simple empirical relationship to calculate coral isotopic ratios from surface ocean isotopic ratios and SSTs is demonstrated to reproduce the variability in coral records at Mahe Island and Maiana Island where precipitation is well simulated, but not at Madang in the western Pacific Warm Pool, where the local ENSO precipitation signal is not reproduced. Where precipitation and isotopic variability is well reproduced by the model, the scheme described here could be used to quantify the relative contribution of SST and local surface ocean isotopic changes to coral isotopic variability. To fully simulate the sensitivity of marine proxies to local conditions, a more complex biophysical model may be necessary. For such studies, the refinements to the surface ocean scheme discussed above would be needed to more accurately simulate the surface ocean isotopic component of the coral oxygen isotope record.

[51] In conclusion, this study demonstrates that a moderate resolution atmospheric GCM incorporating a simple

isotopic surface ocean scheme is able to capture important components of the large-scale temporal and spatial variability of isotopic ratios in tropical precipitation and the surface ocean. Although the model is limited in its ability to reproduce specific isotope records where model resolution or the simulation of precipitation is not sufficiently accurate, it may be used more confidently for large-scale isotopic sensitivity studies. While fully coupled ocean-atmosphere models with isotopic tracers are under development, the approach presented here represents an intermediate approach for simulating surface ocean isotopic variability. As considerable uncertainty remains in the interpretation of tropical isotopic proxy records, the ability to directly simulate the controls on isotopic ratios of both precipitation and the surface ocean can provide an important tool for paleoclimate reconstruction.

[52] **Acknowledgments.** Richard Wardle provided assistance with model development, and Ian Smith offered useful comments on the interpretation of results. Pandora Hope and Kevin Keay provided assistance with data analysis and visualization. The comments of several anonymous reviewers also greatly improved this manuscript. Observational stable water isotope records were obtained from the International Atomic Energy Agency/World Meteorological Organization Global Network of Isotopes in Precipitation (GNIP) database. Ocean isotopic measurements were obtained from the NASA GISS Global Seawater Oxygen-18 Database.

References

- Araguas-Araguas, L., K. Froehlich, and K. Rozanski (1998), Stable isotope composition of precipitation over southeast Asia, *J. Geophys. Res.*, *103*, 28,721–28,742.
- Argete, A., and I. Simmonds (1996), Comparison of temporal cloud variability simulated by a GCM with observations from the NIMBUS-7 satellite, *Atmosfera*, *9*, 1–21.
- Bigg, G. R., and E. J. Rohling (2000), An oxygen isotope data set for marine waters, *J. Geophys. Res.*, *105*, 8527–8535.
- Bradley, R. S., M. Vuille, D. Hardy, and L. G. Thompson (2003), Low latitude ice cores record Pacific sea surface temperatures, *Geophys. Res. Lett.*, *30*(4), 1174, doi:10.1029/2002GL016546.
- Brown, J. (2004), The response of stable water isotopes in precipitation and the surface ocean to tropical climate variability, Ph.D. thesis, Univ. of Melbourne, Melbourne, Victoria, Australia.
- Brown, J., and I. Simmonds (2004), Sensitivity of the $\delta^{18}\text{O}$ -temperature relationship to the distribution of continents, *Geophys. Res. Lett.*, *31*, L09208, doi:10.1029/2004GL019870.
- Charles, C. D., D. Rind, J. Jouzel, R. Koster, and R. Fairbanks (1994), Glacial-interglacial changes in moisture sources for Greenland: Influences on the ice core record of climate, *Science*, *261*, 508–511.
- Charles, C. D., D. E. Hunter, and R. G. Fairbanks (1997), Interaction between the ENSO and the Asian monsoon in a coral record of tropical climate, *Science*, *277*, 925–928.
- Charles, C. D., K. Cobb, M. D. Moore, and R. G. Fairbanks (2003), Monsoon-tropical ocean interaction in a network of coral records spanning the 20th century, *Mar. Geol.*, *201*, 207–222.
- Cobb, K., C. D. Charles, H. Cheng, and R. L. Edwards (2003), El Niño–Southern Oscillation and tropical Pacific climate during the last millennium, *Nature*, *424*, 271–276.
- Cole, J. E., R. G. Fairbanks, and G. T. Shen (1993a), Recent variability in the Southern Oscillation: Isotopic results from a Tarawa Atoll coral, *Science*, *260*, 1790–1793.
- Cole, J. E., D. Rind, and R. G. Fairbanks (1993b), Isotopic responses to interannual climate variability simulated by an atmospheric general circulation model, *Quat. Sci. Rev.*, *12*, 387–406.
- Cole, J. E., D. Rind, R. S. Webb, J. Jouzel, and R. Healy (1999), Climatic controls on interannual variability of precipitation $\delta^{18}\text{O}$: Simulated influence of temperature, precipitation amount, and vapor source region, *J. Geophys. Res.*, *104*, 14,223–14,235.
- Craig, H., and L. I. Gordon (1965), Isotopic oceanography: Deuterium and oxygen 18 variations in the ocean and the marine atmosphere, in *Stable Isotopes in Oceanographic Studies and Paleotemperatures*, edited by E. Tongiorgi, pp. 9–130, Cons. Naz. di Rich., Spoleto, Italy.
- Crowley, T. J., T. M. Quinn, and W. T. Hyde (1999), Validation of coral temperature calibrations, *Paleoceanography*, *14*, 605–615.
- Dansgaard, W. (1964), Stable isotopes in precipitation, *Tellus*, *16*, 436–468.
- Deardorff, J. W. (1977), A parameterization of ground-surface moisture content for use in atmospheric prediction models, *J. Appl. Meteorol.*, *16*, 1182–1185.
- De Deckker, P., N. J. Tapper, and S. van der Kaars (2003), The status of the Indo-Pacific Warm Pool and adjacent land at the Last Glacial Maximum, *Global Planet. Change*, *35*, 25–35.
- Delaygue, G., J. Jouzel, and J. C. Dutay (2000), Oxygen 18-salinity relationship simulated by an oceanic general circulation model, *Earth Planet. Sci. Lett.*, *178*, 113–123.
- Delaygue, G., E. Bard, C. Rollion, J. Jouzel, M. Stievenard, J. C. Duplessy, and G. Ganssen (2001), Oxygen isotope/salinity relationship in the northern Indian Ocean, *J. Geophys. Res.*, *106*, 4565–4574.
- Gagan, M. K., L. K. Ayliffe, J. W. Beck, J. E. Cole, E. R. M. Druffel, R. B. Dunbar, and D. P. Schrag (2000), New views of tropical paleoclimates from corals, *Quat. Sci. Rev.*, *19*, 45–64.
- Gates, W. L., et al. (1999), An overview of the results of the Atmospheric Model Intercomparison Project (AMIP I), *Bull. Am. Meteorol. Soc.*, *80*, 29–55.
- Grootes, P. M., M. Stuiver, L. G. Thompson, and E. Mosley-Thompson (1989), Oxygen isotope changes in tropical ice, Quelccaya, Peru, *J. Geophys. Res.*, *94*, 1187–1194.
- Hoffmann, G. (2003), Taking the pulse of the tropical water cycle, *Science*, *301*, 776–777.
- Hoffmann, G., M. Werner, and M. Heimann (1998), Water isotope module of the ECHAM atmospheric general circulation model: A study on time-scales from days to several years, *J. Geophys. Res.*, *103*, 16,871–16,896.
- Hoffmann, G., et al. (2003), Coherent isotope history of Andean ice cores over the last century, *Geophys. Res. Lett.*, *30*(4), 1179, doi:10.1029/2002GL014870.
- Hut, G. (1987), Consultant's group meeting on stable isotope reference samples for geochemical and hydrological investigations, *Tech. Rep. NTIS DE 87703554*, 42 pp., Int. At. Energy Agency, Vienna.
- Joussame, S., J. Jouzel, and R. Sadourny (1984), A general circulation model of water isotope cycles in the atmosphere, *Nature*, *311*, 24–29.
- Jouzel, J., G. L. Russell, R. J. Suozzo, R. D. Koster, J. W. C. White, and W. S. Broecker (1987), Simulations of the HDO and H₂O atmospheric cycles using the NASA GISS general circulation model: The seasonal cycle for present-day conditions, *J. Geophys. Res.*, *92*, 14,739–14,760.
- Juillet-Leclerc, A., and G. Schmidt (2001), A calibration of the oxygen isotope paleothermometer of coral aragonite from *Porites*, *Geophys. Res. Lett.*, *28*, 4135–4138.
- Juillet-Leclerc, A., J. Jouzel, L. Labeyrie, and S. Joussame (1997), Modern and last glacial maximum sea surface $\delta^{18}\text{O}$ derived from an atmospheric general circulation model, *Earth Planet. Sci. Lett.*, *146*, 591–605.
- Keeling, C. D., T. P. Whorf (2000), Atmospheric CO₂ records from sites in the SIO air sampling network, in *Trends: A Compendium of Data on Global Change*, Carbon Dioxide Inf. Anal. Cent., Oak Ridge Natl. Lab., Oak Ridge, Tenn. (Available at <http://cdiac.esd.ornl.gov/trends/co2/sio-mlo.htm>.)
- Koutavas, A., J. Lynch-Stieglitz, T. M. Marchitto Jr., and J. P. Sachs (2002), El Niño-like pattern in Ice Age tropical Pacific sea surface temperature, *Science*, *297*, 226–230.
- Manabe, S., J. Smagorinsky, and R. Strickler (1965), Simulated climatology of a general circulation model with a hydrologic cycle, *Mon. Weather Rev.*, *93*, 769–798.
- Mathieu, R., D. Pollard, J. E. Cole, J. W. C. White, R. S. Webb, and S. L. Thompson (2002), Simulation of stable water isotopes variations by the GENESIS GCM for modern conditions, *J. Geophys. Res.*, *107*(D4), 4037, doi:10.1029/2001JD900255.
- Noone, D., and I. Simmonds (2002), Associations between $\delta^{18}\text{O}$ of water and climate parameters in a simulation of atmospheric circulation for 1979–1995, *J. Clim.*, *15*, 3150–3169.
- Noone, D., and I. Simmonds (2004), Sea ice control of water isotope transport to Antarctica and implications for ice core interpretation, *J. Geophys. Res.*, *109*, D07105, doi:10.1029/2003JD004228.
- Picaut, J., M. Ioualalen, C. Menkes, T. Delcroix, and M. J. McPhaden (1996), Mechanism of the zonal displacement of the Pacific Warm Pool: Implications for ENSO, *Science*, *274*, 1486–1489.
- Pierrehumbert, R. T. (1999), Huascarán $\delta^{18}\text{O}$ as an indicator of tropical climate during the Last Glacial Maximum, *Geophys. Res. Lett.*, *26*, 1345–1348.
- Poussart, P. F., M. N. Evans, and D. P. Schrag (2004), Resolving seasonality in tropical trees: Multi-decade, high-resolution oxygen and carbon isotope records from Indonesia and Thailand, *Earth Planet. Sci. Lett.*, *218*, 301–316.
- Ramirez, E., et al. (2003), A new Andean deep ice core from Nevado Illimani (6350 m), Bolivia, *Earth Planet. Sci. Lett.*, *212*, 337–350.

- Rayner, N. A., E. B. Horton, D. E. Parker, C. K. Folland, and R. B. Hackett (1996), Version 2.2 of the Global sea-ice and sea surface temperature data set, 1903–1994, *Clim. Res. Tech. Note 74*, Hadley Cent. for Clim. Predict. and Res., Bracknell, U. K.
- Rohling, E. J., and G. R. Bigg (1998), Paleosalinity and $\delta^{18}\text{O}$: A critical assessment, *J. Geophys. Res.*, *103*, 1307–1318.
- Saurer, M., F. Schweingruber, E. A. Vaganov, S. G. Shiyatov, and R. Siegwolf (2002), Spatial and temporal oxygen isotope trends at the northern tree-line in Eurasia, *Geophys. Res. Lett.*, *29*(9), 1296, doi:10.1029/2001GL013739.
- Schimel, D., D. Alves, I. G. Enting, M. Heimann, F. Joos, D. Raynaud, and T. M. L. Wigley (1996), CO_2 and the carbon cycle, in *Climate Change 1995: The Science of Climate Change*, edited by J. T. Houghton et al., pp. 76–86, Cambridge Univ. Press, New York.
- Schmidt, G. A. (1998), Oxygen-18 variations in a global ocean model, *Geophys. Res. Lett.*, *25*, 1201–1204.
- Schmidt, G. A. (1999a), Error analysis of paleosalinity calculations, *Paleoceanography*, *14*, 422–429.
- Schmidt, G. A. (1999b), Forward modeling of carbonate proxy data from planktonic foraminifera using oxygen isotope tracers in a global ocean model, *Paleoceanography*, *14*, 482–497.
- Simmonds, I. (1985), Analysis of the “spinup” of a general circulation model, *J. Geophys. Res.*, *90*, 5637–5660.
- Stott, L., C. Poulsen, S. Lund, and R. Thunell (2002), Super ENSO and global climate oscillations at millennial time scales, *Science*, *297*, 222–226.
- Thompson, L. G. (2000), Ice core evidence for climate change in the tropics: Implications for our future, *Quat. Sci. Rev.*, *19*, 19–35.
- Thompson, L. G., E. Mosley-Thompson, J. F. Bolzan, and B. R. Koci (1985), A 1500-year record of tropical precipitation in ice cores from Quelccaya ice cap, Peru, *Science*, *229*, 971–973.
- Thompson, L. G., E. Mosley-Thompson, M. E. Davis, J. F. Bolzan, J. Dai, T. Yao, N. Gundestrup, X. Wu, L. Klein, and Z. Yie (1989), Holocene–late Pleistocene climatic ice core records from Qinghai-Tibetan Plateau, *Science*, *246*, 474–477.
- Thompson, L. G., E. Mosley-Thompson, M. E. Davis, P.-N. Lin, K. A. Henderson, and J. Cole-Dai (1995), Late glacial stage and Holocene tropical ice core records from Huascarán, Peru, *Science*, *269*, 46–50.
- Thompson, L. G., T. Yao, M. E. Davis, K. A. Henderson, E. Mosley-Thompson, P.-N. Lin, J. Beer, H.-A. Synal, J. Cole-Dai, and J. F. Bolzan (1997), Tropical climate instability: The last glacial cycle from a Qinghai-Tibetan ice core, *Science*, *276*, 1821–1825.
- Thompson, L. G., et al. (1998), A 25,000 year tropical climate record from Bolivian ice cores, *Science*, *282*, 1858–1864.
- Thompson, L. G., E. Mosley-Thompson, and K. A. Henderson (2000a), Ice-core palaeoclimate records in tropical South America since the Last Glacial Maximum, *J. Quat. Sci.*, *15*, 377–394.
- Thompson, L. G., T. Yao, E. Mosley-Thompson, M. E. Davis, K. A. Henderson, and P.-N. Lin (2000b), A high-resolution millennial record of the south Asian monsoon from Himalayan ice cores, *Science*, *289*, 1916–1919.
- Thompson, L. G., et al. (2002), Kilimanjaro ice core records: Evidence of Holocene climate change in tropical Africa, *Science*, *298*, 589–593.
- Thompson, L. G., E. Mosley-Thompson, M. E. Davis, P.-N. Lin, K. A. Henderson, and T. A. Mashiotto (2003), Tropical glacier and ice core evidence of climate change on annual to millennial time scales, *Clim. Change*, *59*, 137–155.
- Tian, L., V. Masson-Delmotte, M. Stievenard, T. Yao, and J. Jouzel (2001), Tibetan Plateau summer monsoon northward extent revealed by measurements of water stable isotopes, *J. Geophys. Res.*, *106*, 28,081–28,088.
- Tudhope, A. W., G. B. Shimmield, C. P. Chilcott, M. Jebb, A. E. Fallick, and A. N. Dalglish (1995), Recent changes in climate in the far western equatorial Pacific and their relationship to the Southern Oscillation: Oxygen isotope records from massive corals, Papua New Guinea, *Earth Planet. Sci. Lett.*, *136*, 575–590.
- Tudhope, A. W., C. P. Chilcott, M. T. McCulloch, E. R. Cook, J. Chappell, R. M. Ellam, D. W. Lea, J. M. Lough, and G. B. Shimmield (2001), Variability in the El Niño–Southern Oscillation through a glacial-interglacial cycle, *Science*, *291*, 1511–1517.
- Urban, F. E., J. E. Cole, and J. T. Overpeck (2000), Influence of mean climate change on climate variability from a 155-year tropical Pacific coral record, *Nature*, *407*, 989–993.
- Valdes, P. J. (2000), South American palaeoclimate model simulations: How reliable are the models?, *J. Quat. Sci.*, *15*, 357–368.
- von Storch, H., and F. W. Zwiers (1999), *Statistical Analysis in Climate Research*, 494 pp., Cambridge Univ. Press, New York.
- Vuille, M., R. S. Bradley, M. Werner, R. Healy, and F. Keimig (2003a), Modeling $\delta^{18}\text{O}$ in precipitation over the tropical Americas: 1. Interannual variability and climatic controls, *J. Geophys. Res.*, *108*(D6), 4174, doi:10.1029/2001JD002038.
- Vuille, M., R. S. Bradley, R. Healy, M. Werner, and D. R. Hardy (2003b), Modeling $\delta^{18}\text{O}$ in precipitation over the tropical Americas: 2. Simulation of the stable isotope signal in Andean ice cores, *J. Geophys. Res.*, *108*(D6), 4175, doi:10.1029/2001JD002039.
- Wadley, M. R., G. R. Bigg, E. C. Rohling, and A. J. Payne (2002), On modelling present-day and last glacial maximum $\delta^{18}\text{O}$ distributions, *Global Planet. Change*, *32*, 89–109.
- Wellington, G. M., R. B. Dunbar, and G. Merlen (1996), Calibration of stable oxygen isotope signatures in Galápagos coral, *Paleoceanography*, *11*, 467–480.
- Williamson, D. L., and P. J. Rasch (1989), Two-dimensional semi-Lagrangian transport with shape-preserving interpolation, *Mon. Weather Rev.*, *117*, 102–129.
- Xie, P., and P. A. Arkin (1996), Analysis of global monthly precipitation using gauge observations, satellite estimates, and numerical model predictions, *J. Clim.*, *9*, 840–858.
- Yao, T., L. G. Thompson, E. Mosley-Thompson, Z.-H. Yang, X.-P. Zhang, and P.-N. Lin (1996), Climatological significance of $\delta^{18}\text{O}$ in north Tibetan ice cores, *J. Geophys. Res.*, *101*, 29,531–29,537.

J. Brown, Centre for Global Atmospheric Modeling, Department of Meteorology, University of Reading, Earley Gate, PO Box 243, Reading RG6 6BB, UK. (josephine.brown@reading.ac.uk)

D. Noone, Program in Atmospheric and Oceanic Sciences and Cooperative Institute for Research in Environmental Sciences, University of Colorado, Boulder, CO 80303, USA.

I. Simmonds, School of Earth Sciences, University of Melbourne, Parkville, Vic 3010, Australia.